

October 17, 2018

Transverse phase-locking in fully frustrated Josephson junction arrays: a new type of fractional giant steps

Verónica I. Marconi

The Abdus Salam International Centre for Theoretical Physics, I-34014, Trieste, Italy

Alejandro B. Kolton and Daniel Domínguez

Centro Atómico Bariloche, 8400 San Carlos de Bariloche, Río Negro, Argentina.

Niels Grønbech-Jensen

Department of Applied Science, University of California, Davis, California 95616

and Computational Research Division, Lawrence Berkeley National Laboratory, Berkeley, California 94720.

We study, analytically and numerically, phase locking of driven vortex lattices in fully-frustrated Josephson junction arrays at zero temperature. We consider the case when an ac current is applied *perpendicular* to a dc current. We observe phase locking, steps in the current-voltage characteristics, with a dependence on external ac-drive amplitude and frequency qualitatively different from the Shapiro steps, observed when the ac and dc currents are applied in parallel. Further, the critical current increases with increasing transverse ac-drive amplitude, while it decreases for longitudinal ac-drive. The critical current and the phase-locked current step width, increase quadratically with (small) amplitudes of the ac-drive. For larger amplitudes of the transverse ac-signal, we find windows where the critical current is hysteretic, and windows where phase locking is suppressed due to dynamical instabilities. We characterize the dynamical states around the phase-locking interference condition in the IV curve with voltage noise, Lyapunov exponents and Poincaré sections. We find that zero temperature phase-locking behavior in large fully frustrated arrays is well described by an effective four plaquette model.

PACS numbers: PACS numbers: 74.81.Fa, 74.25.Sv, 74.25.Qt

I. INTRODUCTION

Phase locking phenomena are found in a wide variety of nonlinear driven systems in condensed matter physics.¹ It takes place when an internal frequency of the system locks to a rational multiple of the frequency of an external ac-drive. A simple example of this is the case of an overdamped particle moving in a tilted washboard potential, where the frequency of motion of the particle over the periodic potential can be locked to multiples of the frequency of a superimposed ac force for a finite range of the dc force (tilt of the washboard). Since the internal (washboard) frequency is proportional to the mean velocity of the particle, phase locking results in a constant mean velocity for a certain range of dc-force curve when the interference condition is satisfied. A particularly well known realization of this effect is Shapiro steps² in the dc current-voltage (IV) characteristics of a single small area Josephson junction driven by a time periodic current. Within the washboard analogy outlined above, a simple analysis provides expressions for the appearance of Shapiro steps at specific voltages³ corresponding to integer multiples of the driving frequency.

Driven systems with many degrees of freedom can also exhibit phase locking. This has attracted broad scientific and technological interest since phase-locking in complex systems can either be induced by collective effects, providing for a low dimensional interpretation of the phenomenon, or itself induce collective (low dimensional) behavior in the complex system. Phase-locking experiments have provided information about such dynamical response of non-equilibrium collective states, where dimensionality, thermal fluctuations, quenched disorder, and the magnitude of external fields can be very relevant. A particular well known example is the large Josephson junction array (JJA), with $N \times N$ junctions, driven by an external current $(I_{dc} + I_{ac} \cos \Omega t)\hat{x}$ with frequency Ω and with an applied magnetic field density $f = Ha^2/\Phi_0$, where H is the magnetic field, a the lattice period of the Josephson array and Φ_0 the quantum of flux. *Giant* Shapiro steps at voltages $V_n = Nn\hbar\Omega/2e$, n being an integer, have been observed experimentally in zero magnetic field ($f = 0$).⁴ *Fractional giant* Shapiro steps at voltages $V_{n,q} = Nn\hbar\Omega/2eq$, were observed experimentally^{5,6} for strongly commensurate magnetic fields, $f = p/q$, with p, q integers, and extensively investigated in numerical simulations.^{7,8,9,10,11} Also, *subharmonic* giant Shapiro steps at voltages $V_{n,m} = Nn\hbar\Omega/2em$ were observed experimentally⁶ for zero magnetic field ($f = 0$), and attributed to the nucleation of complex collective dynamical states^{12,13} induced by disorder or inductance effects. Shapiro-like phase-locking is also observed in the case of driven vortex lattices in bulk superconductors with two-dimensional periodic pinning arrays, as recently reported both experimentally¹⁴ and theoretically.¹⁵ Also superconductors, where vortices are driven over a one-dimensional

potential generated by thickness modulations,¹⁶ or are confined to move through mesoscopic channels,¹⁷ show Shapiro-like phase-locking. Moreover, systems with many degrees of freedom in the presence of quenched disorder can also exhibit phase-locking when there is a dynamically induced periodicity, like charge density waves¹⁸ and vortex lattices in superconductors with random pinning.^{19,20,21}

In the phase-locking examples mentioned above, the ac-drive is applied parallel to the dc-drive. However, it was recently shown that a different type of phase-locking, distinct from Shapiro phase-locking, is possible in vortex lattices if the ac-force is applied *perpendicular* to the dc-force.^{22,23} In this case the interference effect is due to an effective *parametric* ac drive in the longitudinal direction, which is induced by the transverse ac drive. In several systems, like charge density waves or single degree of freedom systems (*e.g.*, the single Josephson junction), the dynamical variables are such that perturbations or displacements can be induced in only one direction (*i.e.*, the displacement field is a scalar). An important characteristic of vortex lattices in superconductors is that the displacement field is two dimensional. In particular, the behavior of displacements in the direction perpendicular to the driving force shows phenomena like a transverse critical current^{24,25,26,27} and a transverse freezing transition^{24,28} at high velocities. Phase locking in ac-driven vortex lattices, where the ac and dc forces are perpendicular, arises as a direct consequence of the nonlinear coupling between the two directions of motions.

Transverse phase-locking has been reported for vortex lattices moving in rectangular or triangular pinning arrays²² as well as in arrays of randomly distributed pinning centers.²³ In this paper we investigate the possibility of transverse phase locking in a two dimensional (2D) fully frustrated JJA, where the average of the external magnetic field corresponds to one half flux quantum per plaquette, $f = 1/2$. This system has several attractive properties. The presence of a magnetic field ($f \neq 0$) breaks the axial symmetry in the direction of the bias current, and 2D-cooperative behavior may come into play. This leads to the well-known fractional giant Shapiro steps^{5,6,7,8,9,10,11} induced by a longitudinal ac current. It also, as we will demonstrate in this paper, allows for *transverse* phase locking when the ac current is perpendicular to the dc current, since the two directions of motion become coupled. Non-equilibrium dynamical phases for fully frustrated JJAs driven by a dc current have previously been studied.^{29,30} Phase locking can be used to characterize temporal order in the different dynamical phases of the JJA at high velocities by their ac-response, as was done in Ref. 20,21 for bulk superconductors.

Here, we report transverse phase locking steps in the IV characteristics, similar to the longitudinal giant Shapiro steps, but with very different characteristic dependencies on external ac-drive amplitude I_{ac} and frequency Ω . The critical depinning current in the system with transverse ac drive is *larger* than the critical current of the dc driven system. For $I_{ac}/\Omega \ll 1$ the depinning critical current I_c and the phase-locked step width ΔS_1 for $V = \Omega\hbar/2e$ increase quadratically with I_{ac} . For $I_{ac}/\Omega > 1$ we find windows of I_{ac}/Ω where depinning is hysteretic and the periodic phase-locked dynamical states become unstable. We characterize the dynamical states around the phase-locking interference condition in the IV curve with the voltage noise, Lyapunov exponents and Poincaré sections. We find that zero temperature phase-locking behavior in large fully frustrated arrays is well described by an effective four plaquette model.

The remainder of this paper is outlined as follows. In section II we present the model used for simulating the dynamics of the fully frustrated JJA. In section III we develop an analytical framework for predicting critical current and phase-locking properties of the fully frustrated JJA. Section IV presents simulated transverse phase-locking steps in typical IV curves obtained from an effective four plaquette model for the JJA. We calculate numerically the dependence of the critical current and the magnitude of phase-locking steps with the amplitude I_{ac} and frequency Ω of the external ac-drive. The results obtained are analyzed in more detail by studying voltage noise, Lyapunov exponents and Poincaré sections for the dynamical states around the phase-locking interference condition. We also compare numerical simulations results for large arrays with those obtained using the effective four plaquette model. The discussions and conclusions of the investigation are presented in sections IV and V.

II. MODEL

We study a current driven JJA with an ac current perpendicular to the dc current, as shown in figure 1a. A magnetic field, H , is applied such that half a flux quantum, $f = Ha^2/\Phi_0 = 1/2$ with a^2 being the area of a plaquette and $\Phi_0 = h/2e$ being the flux quantum, penetrates each plaquette; corresponding to the fully frustrated XY model,^{31,32} where the ground state is a “checkerboard” vortex lattice, in which a vortex (flux quantum) penetrates every other square grid (see Fig. 1b). In such ground state, current and phase differences in the junctions are described by a repeated two-junction by two-junction (2×2 plaquette) superlattice unit cell.

Numerical simulations^{7,8} of large driven arrays suggest that this spatial periodicity is preserved when the dynamics is phase-locked to an external ac-perturbation applied in parallel to the dc force. We will show later, in section IV, that this is also a good approximation when the ac current is *perpendicular* to the dc current. We will therefore consider the simple system of a 2×2 superlattice unit cell of the array and the associated gauge-invariant phase

differences in a field of $f = 1/2$, with the dc current (per plaquette) I_{dc} perpendicular to an ac current (per plaquette) $I_{ac} \cos(\Omega t)$, as shown in Fig. 2. Flux quantization, total current conservation at the central node, and the applied total currents in the two directions give the following governing equations,

$$\alpha + \beta - \delta - \gamma = \pi(1 + 2n) \quad (1)$$

$$\dot{\beta} + \dot{\gamma} + \sin \beta + \sin \gamma = 2I_{ac} \cos \Omega t \quad (2)$$

$$\dot{\alpha} + \dot{\delta} + \sin \alpha + \sin \delta = 2I_{dc} \quad (3)$$

$$\dot{\alpha} + \dot{\gamma} - \dot{\beta} - \dot{\delta} + \sin \alpha + \sin \gamma - \sin \beta - \sin \delta = 0, \quad (4)$$

where n is an integer, t is the normalized time in units of $t_0 = 2eI_0R_N/\hbar$, R_N being the normal state single junction resistance, Ω is the normalized frequency in units of $1/t_0$, I_{ac} and I_{dc} are the normalized external currents in units of the single junction critical current I_0 . This model was introduced by Benz *et al.*³³ (for $I_{ac} = 0$) to study the dc current-voltage curve of the $f = 1/2$ array. They obtained analytically that the critical current per junction of this model is $I_c = (\sqrt{2} - 1)I_0$.³³ The same model was later used in Ref. 9 to study the (longitudinal) Shapiro steps. Since the analysis done in the work of Refs. 9,33 did not include the transverse ac current with accompanying transverse voltage drop, an additional constraint of $\beta = \delta$ was implied, reducing the model system to two dynamical degrees of freedom. In contrast, our model system of a four plaquette unit cell consists of three effective dynamical variables. We calculate the instantaneous longitudinal V_x and transverse V_y (normalized) voltages per junction as,

$$V_x = (\dot{\alpha} + \dot{\delta})/2 \quad (5)$$

$$V_y = (\dot{\beta} + \dot{\gamma})/2, \quad (6)$$

and the IV characteristics, $v_x = \langle V_x \rangle$ as a function of I_{dc} , where $\langle \dots \rangle$ is a time average. The total longitudinal voltage v_T for an $N \times N$ array, built with this 2×2 superlattice unit cell, is $v_T = Nv_x$. When vortices move with a mean velocity u in such $2a \times 2a$ superlattice structure, we can obtain the normalized voltage v_x using the relation $2\pi u/2a = v_x$, where a is the array periodicity (see Fig. 1a). The intrinsic washboard frequency for vortices moving with velocity u in the periodic potential of the JJA is $\omega_0 = 2\pi u/a$. Phase-locking in the longitudinal direction is obtained when the frequency Ω of the ac drive locks to a rational multiple of the intrinsic washboard frequency. For the n -th harmonic this corresponds to $\omega_0 = n\Omega$, *i.e.* $2\pi u/a = n\Omega$. This leads to phase-locking at voltages $V_{n,2} = (n/2)\Omega$ for fully frustrated JJA. In general, for $f = p/q$, the ground state has $qa \times qa$ superlattice structure, therefore the voltage for vortices moving with velocity u is $2\pi u/qa = v_x$, and phase-locking for the n -th harmonic is obtained at voltages $V_{n,q} = (n/q)\Omega$. This is the condition for the so-called ‘‘fractional giant Shapiro steps’’^{5,6,7,8,9,10,11}.

III. PHASE-LOCKING AND CRITICAL CURRENT ANALYSIS

We will in this section assume that the dynamics of the system is represented by the simple two-plaquette degrees of freedom as shown in figure 2. We will apply the following linear transformation of the phase-variables of Eqs. (1)-(4):

$$\Phi_x = \frac{\alpha + \delta}{2} \quad (7)$$

$$\Psi_x = \frac{\alpha - \delta}{2} \quad (8)$$

$$\Phi_y = \frac{\beta + \gamma}{2} \quad (9)$$

$$\Psi_y = \frac{\beta - \gamma}{2}. \quad (10)$$

With these variables we can represent the constraint ($f = 1/2$) of Eq. (1) as $\Psi_x + \Psi_y = \frac{\pi}{2}$, and thereby write the relevant three degrees of freedom in either of the two following forms, eliminating Ψ_x :

$$\dot{\Phi}_x + \sin \Psi_y \sin \Phi_x = I_{dc} \quad (11)$$

$$\dot{\Phi}_y + \cos \Psi_y \sin \Phi_y = I_{ac} \cos \Omega t \quad (12)$$

$$2\dot{\Psi}_y - \cos \Phi_x \cos \Psi_y + \cos \Phi_y \sin \Psi_y = 0, \quad (13)$$

or eliminating Ψ_y :

$$\dot{\Phi}_x + \cos \Psi_x \sin \Phi_x = I_{dc} \quad (14)$$

$$\dot{\Phi}_y + \sin \Psi_x \sin \Phi_y = I_{ac} \cos \Omega t \quad (15)$$

$$2\dot{\Psi}_x + \cos \Phi_x \sin \Psi_x - \cos \Phi_y \cos \Psi_x = 0. \quad (16)$$

The normalized voltages are given by, $V_x = \dot{\Phi}_x$ and $V_y = \dot{\Phi}_y$. We will in the spirit of the usual Shapiro analysis assume that

$$\Phi_y = \frac{I_{ac}}{\Omega} \sin \Omega t, \quad (17)$$

which is the solution to Eqs. (12) and (15) for large I_{ac} and Ω .

A. Critical Current

We will here look at Eqs. (14) and (16). Assuming $\Phi_x = \Phi_x^{(0)}$ and $\Psi_y = \Psi_y^{(0)} + \varepsilon(t)$, where $\Phi_x^{(0)}$ and $\Psi_y^{(0)}$ are constants and $|\varepsilon(t)| \ll 1$, the static contribution to equation (16) is:

$$\cos \Phi_x^{(0)} \sin \Psi_y^{(0)} = J_0 \left(\frac{I_{ac}}{\Omega} \right) \cos \Psi_y^{(0)} \quad (18)$$

$$\Rightarrow \tan \Psi_y^{(0)} = \frac{J_0 \left(\frac{I_{ac}}{\Omega} \right)}{\cos \Phi_x^{(0)}}, \quad (19)$$

where J_n is the n 'th order Bessel function of the first kind. Inserting this into the static part of equation (14) yields

$$I_{dc} = \cos \left\{ \tan^{-1} \left[\frac{J_0 \left(\frac{I_{ac}}{\Omega} \right)}{\cos \Phi_x^{(0)}} \right] \right\} \sin \Phi_x^{(0)}. \quad (20)$$

This expression provides a unique relationship between the constant phase, $\Phi_x^{(0)}$, and the dc current, I_{dc} . However, for increasing I_{dc} , there exists a critical value, I_c^\dagger , for which no real $\Phi_x^{(0)}$ can satisfy Eq. (20). This value is given by

$$I_c^\dagger = \max \left[\cos \left\{ \tan^{-1} \left[\frac{J_0 \left(\frac{I_{ac}}{\Omega} \right)}{\cos \Phi_x^{(0)}} \right] \right\} \sin \Phi_x^{(0)} \right], \quad (21)$$

which is the predicted critical dc current for static states ($v_x = \langle \dot{\Phi}_x \rangle = 0$). We notice that the identical expression for the critical current, Eq. (21), can be obtained from the *anisotropic* dc driven system,

$$\alpha + \beta - \delta - \gamma = \pi(1 + 2n) \quad (22)$$

$$\dot{\beta} + \dot{\gamma} + \Gamma \sin \beta + \Gamma \sin \gamma = 0 \quad (23)$$

$$\dot{\alpha} + \dot{\delta} + \sin \alpha + \sin \delta = 2I_{dc} \quad (24)$$

$$\dot{\alpha} + \dot{\gamma} - \dot{\beta} - \dot{\delta} + \sin \alpha + \Gamma \sin \gamma - \Gamma \sin \beta - \sin \delta = 0, \quad (25)$$

where the anisotropy, Γ (suppression of transverse critical current), is given by the standard Shapiro³ critical current, $\Gamma = J_0 \left(\frac{I_{ac}}{\Omega} \right)$.

B. Phase-Locking

We will here use equations (11)-(13), since $\langle \Psi_y \rangle = 0 \pmod{\pi}$ for $\langle \dot{\Phi}_x \rangle \neq 0$ provides for a simple description of the dynamics. We will assume the ansatz, $\Phi_x = \Phi_x^{(0)} + \Omega t$ and $\Psi_y = A \sin \Omega t + B \cos \Omega t$. The equation for Ψ_y , (13), now reads:

$$2\dot{\Psi}_y - \cos(\Phi_x^{(0)} + \Omega t) \cos \Psi_y + \sin \Psi_y \sum_k J_k \left(\frac{I_{ac}}{\Omega} \right) \cos k\Omega t = 0, \quad (26)$$

where we will use the approximations: $\cos \Psi_y \approx J_0(\sqrt{A^2 + B^2})$ and $\sin \Psi_y \approx \Psi_y$. With the ansatz for Ψ_y above, this equation has no static component. The time varying component, at frequency Ω , yields the coefficients A and B

$$A_1 = A_0 J_0 \left(\sqrt{A_0^2 + B_0^2} \right) = \frac{2\Omega \cos \Phi_x^{(0)} - [J_0 \left(\frac{I_{ac}}{\Omega} \right) + J_2 \left(\frac{I_{ac}}{\Omega} \right)] \sin \Phi_x^{(0)}}{4\Omega^2 + J_0^2 \left(\frac{I_{ac}}{\Omega} \right) - J_2^2 \left(\frac{I_{ac}}{\Omega} \right)} J_0 \left(\sqrt{A_0^2 + B_0^2} \right) \quad (27)$$

$$B_1 = B_0 J_0 \left(\sqrt{A_0^2 + B_0^2} \right) = \frac{2\Omega \sin \Phi_x^{(0)} + [J_0 \left(\frac{I_{ac}}{\Omega} \right) - J_2 \left(\frac{I_{ac}}{\Omega} \right)] \cos \Phi_x^{(0)}}{4\Omega^2 + J_0^2 \left(\frac{I_{ac}}{\Omega} \right) - J_2^2 \left(\frac{I_{ac}}{\Omega} \right)} J_0 \left(\sqrt{A_0^2 + B_0^2} \right), \quad (28)$$

where A_0 and B_0 are the solutions for $J_0 \left(\sqrt{A_0^2 + B_0^2} \right) = 1$. Thus, the solution $(A, B) = (A_0, B_0)$ is correct up to order Ω^{-1} and $(A, B) = (A_1, B_1)$ is correct up to Ω^{-2} . Inserting this solution (A_1, B_1) for Ψ_y into the Ψ_y -linearized equation (11) gives the static properties:

$$J_0 \left(\sqrt{A_0^2 + B_0^2} \right) \frac{1}{2} \left(A_0 \cos \Phi_x^{(0)} + B_0 \sin \Phi_x^{(0)} \right) = I_{dc} - \Omega \Rightarrow \quad (29)$$

$$\begin{aligned} J_0 \left(\sqrt{A_0^2 + B_0^2} \right) \frac{1}{2} \frac{2\Omega - J_2 \left(\frac{I_{ac}}{\Omega} \right) \sin 2\Phi_x^{(0)}}{4\Omega^2 + J_0^2 \left(\frac{I_{ac}}{\Omega} \right) - J_2^2 \left(\frac{I_{ac}}{\Omega} \right)} &\approx \Delta I_1 - \frac{1}{2} \Delta S_1 \sin 2\Phi_x^{(0)} \\ &= I_{dc} - \Omega. \end{aligned} \quad (30)$$

Thus, the locking range for the this step can be found to second order in $|\Psi_y|$. The dominant part of this expression for the range in phase-locking yields:

$$\Delta S_1 = \frac{\left| J_2 \left(\frac{I_{ac}}{\Omega} \right) \right|}{4\Omega^2 + J_0^2 \left(\frac{I_{ac}}{\Omega} \right) - J_2^2 \left(\frac{I_{ac}}{\Omega} \right)} \left(1 - \frac{3\Omega^2 + \frac{1}{4} (J_0^2 \left(\frac{I_{ac}}{\Omega} \right) + J_2^2 \left(\frac{I_{ac}}{\Omega} \right))}{(4\Omega^2 + J_0^2 \left(\frac{I_{ac}}{\Omega} \right) - J_2^2 \left(\frac{I_{ac}}{\Omega} \right))^2} \right). \quad (31)$$

The expression displays quadratic growth of the phase-locked step size for small I_{ac} . This is consistent with the particle (pancake) model results²² for vortices in rectangular pinning arrays, and it is different from the known longitudinal (Shapiro) phase-locking of JJAs.^{4,5,6,7}

In addition to the range of phase-locking, ΔS_1 , equation (30) provides information about the offset, ΔI_1 , of the phase-locked step relative to the Ohmic (linear) curve (see inset in figure 3). The offset is given by the part of the equation that does *not* depend on $\Phi_x^{(0)}$. From Eq. (30) we have:

$$\Delta I_1 = \frac{\Omega}{4\Omega^2 + J_0^2 \left(\frac{I_{ac}}{\Omega} \right) - J_2^2 \left(\frac{I_{ac}}{\Omega} \right)} \left(1 - \frac{1}{4} \frac{4\Omega^2 + J_0^2 \left(\frac{I_{ac}}{\Omega} \right) + 2J_2^2 \left(\frac{I_{ac}}{\Omega} \right)}{(4\Omega^2 + J_0^2 \left(\frac{I_{ac}}{\Omega} \right) - J_2^2 \left(\frac{I_{ac}}{\Omega} \right))^2} \right). \quad (32)$$

Expressions (31) and (32) provide a second order (in Ω^{-1}) description of the phase-locking step magnitude and location as a function of the system parameters, Ω and I_{ac} , for large Ω .

IV. RESULTS AND DISCUSSION

We will here show the results of numerical simulations of the system analyzed in the previous section. The simulations are conducted with numerical parameters corresponding to the model parameters, using a fourth order Runge-Kutta method such that the normalized time step typically is no larger than 1% of the period of the driving frequency, and often smaller. Since we are mostly concerned with dc IV characteristics, we choose to acquire data for averaging over many ac-periods of motion (typically 10^2 - 10^3) after a sufficient initial time of interval allowed for transient behavior. Simulated IV characteristics are obtained by performing the necessary averages as described, and then changing the dc current, I_{dc} , slightly to acquire the next point on the IV curve. All simulations are conducted for the fully frustrated case of $f = \frac{1}{2}$.

Figure 3 shows a simulated IV characteristic, v_x as a function of I_{dc} , simulated for $\Omega = 1$ and $I_{ac} = 2.3$, for the simple four plaquette model showed in figure 2, described by the equations (1)-(4). As is obvious from the figure, we obtain clear signatures of critical current(s) and phase-locked steps. Specifically, we observe the ΔS_1 step at $v_x = \Omega$, and steps $\Delta S_{\frac{1}{2}}$ and ΔS_2 at $v_x = \frac{1}{2}\Omega$ and $v_x = 2\Omega$, respectively. We observe a critical current larger than the previously predicted³³ value of $I_c = \sqrt{2} - 1 \approx 0.41$ for a fully frustrated dc-driven system. The characteristics of this plot are very similar to the behavior observed in JJA with parallel ac + dc drives, obtained both by simulations^{8,10} and experiments,⁵ as well as analytically for the four plaquette model.⁹

Comparing simulations of the full-RSJ dynamical equations^{27,30} for different large arrays ($N \times N$ junctions) we will later (below) demonstrate that the simple model of a 2×2 array gives very good description of the JJA dynamics. However, we will first compare the predictions of the analytical treatment of the previous section to numerical results.

A. Critical Current and Phase-Locking for $\Omega \geq 1$

In order to verify the simple theory for critical current and phase-locking behavior developed above, we have conducted numerical simulations of the four plaquette system described by Eqs. (1)-(4) for $1 \leq \Omega$.

The first set of simulations are conducted to investigate the critical current, I_c , as it is described by Eq. (21). This expression provides an estimate of the critical current, I_c^\uparrow , for which the JJA switches from a zero-voltage state ($\langle V_x \rangle = 0$ and $I_{dc} < I_c^\uparrow$) to a non-zero voltage state. The simulations are conducted accordingly, starting the system at rest for small I_{dc} and slowly increasing the dc-bias until non-zero average voltage is detected. The results are shown in figure 4a, where the solid curve represents the expression, Eq. (21), and the markers represent the simulation results for several frequencies $1 \leq \Omega \leq 3$ as a function of the characteristic ratio, $\frac{I_{ac}}{\Omega}$. The size of the markers are larger than the error on the estimated critical current. It is obvious that the agreement is very good for all simulated data sets, and we conclude that the critical current, as given by Eq. (21), is a relevant estimate for Ω not smaller than 1.

Figure 4b shows the critical current, I_c^\downarrow , evaluated from numerical simulations when the dynamical system switches from the non-zero voltage state to the zero-voltage state (see inset in figure 3). We have here shown the results of numerical simulations with markers as for figure 4a, together with the solid curve of Eq. (21). However, it is clear from the figure that the critical current, I_c^\downarrow , for decreasing dc-bias may be smaller than for increasing dc-bias ($I_c^\uparrow \geq I_c^\downarrow$). Since this is a multi-dimensional system, the critical current may be hysteretic, such that decreasing the dc-current, I_{dc} , for non-zero voltage states ($v_x = \langle \dot{\Phi}_x \rangle \neq 0$) is subject to different critical characteristics. One simple way of investigating this is to assume a non-phase-locked state of voltage $v_x \neq 0$, such that $\Phi_x = v_x t$. A primitive analysis can provide a hint to this hysteresis.

The critical current analysis of the previous section, is obviously a critical current for a system operated at the $\langle \dot{x} \rangle = 0$ branch of the IV -curve. We may instead analyze what may happen for a *non-phase-locked* $\langle \dot{\Phi}_x \rangle = v_x \neq 0$ state. We will still assume (17) to be an appropriate description of the transverse current. However, equation (13) becomes (for small $|\Psi_y|$ and with no resonance to Ω):

$$2\dot{\Psi}_y - \cos v_x t + J_0 \left(\frac{I_{ac}}{\Omega} \right) \Psi_y = 0 \quad (33)$$

$$\Rightarrow \Psi_y = \frac{J_0 \left(\frac{I_{ac}}{\Omega} \right)}{J_0^2 \left(\frac{I_{ac}}{\Omega} \right) + 4v_x^2} \cos v_x t + \frac{2v_x}{J_0^2 \left(\frac{I_{ac}}{\Omega} \right) + 4v_x^2} \sin v_x t. \quad (34)$$

Inserting the Ψ_y solution into equation (11) yields the static component:

$$v_x + \left| J_1 \left(\frac{2v_x}{J_0^2 \left(\frac{I_{ac}}{\Omega} \right) + 4v_x^2} \right) \right| = I_{dc}, \quad (35)$$

where the second term on the left hand side is the result of the resonant mixing between the propagation, $\langle \dot{\Phi}_x \rangle = v_x$ and the transverse oscillation, Ψ_y . However, the overdamped dc driven pendulum equation is also subject to the following simple relationship,³

$$\sqrt{v_x^2 + (I_c^\downarrow)^2} = I_{dc}. \quad (36)$$

Combining the two expressions provides the relationship

$$I_c^\downarrow = \sqrt{\left[v_x + \left| J_1 \left(\frac{2v_x}{J_0^2 \left(\frac{I_{ac}}{\Omega} \right) + 4v_x^2} \right) \right| \right]^2 - v_x^2} \leq 0.826591. \quad (37)$$

As we have indicated, the critical current, I_c^\downarrow has a maximum value at around 0.82 (for $J_0 \left(\frac{I_{ac}}{\Omega} \right) = 0$ and $v_x \approx 0.33$). Thus, we can argue that propagating ($\langle \dot{\Phi}_x \rangle \neq 0$) solutions may exist for $I_{dc} > I_c^\downarrow \approx 0.82$, which provides for a hysteretic IV characteristic switching between zero and non-zero voltages in the range $I_c^\downarrow \leq I_{dc} \leq I_c^\uparrow$, when $I_c^\downarrow \leq I_c^\uparrow$. Notice that when $I_c^\downarrow > I_c^\uparrow$, the relevant critical current for both zero and non-zero voltage states must be I_c^\uparrow , since no static states exist for $I_{dc} > I_c^\uparrow$. However, when $I_c^\downarrow < I_c^\uparrow$, the actual critical current for switching into a zero-voltage state may be anywhere in the interval $[I_c^\downarrow; I_c^\uparrow]$.

Figure 4 clearly indicates the hysteretic switching in the IV characteristics when $I_c^\downarrow \leq I_{dc} \leq I_c^\uparrow$, which is the case for small $|J_0(\frac{I_{ac}}{\Omega})|$.

We note that the above rather primitive analysis of the hysteresis provides a fairly good agreement with the results of numerical simulations. The results of the analysis are not completely consistent with its assumptions in that the resulting amplitude of Ψ_y for the optimized $v_x \approx 0.33$ is about 1.5, which is not a small number. However, a more detailed (nonlinear) analysis of a single frequency representation of Ψ_y yields quantitatively similar and qualitatively identical results ($I_c^\downarrow \leq 0.77$) as the above, and we therefore conclude that the simple explanation for hysteresis presented here is relevant.

For $J_0(\frac{I_{ac}}{\Omega}) = 0$ we can provide an explicit approximate expression for I_c^\downarrow by assuming the critical current is given by the value of v_x which optimizes $J_1(\frac{1}{2v_x})$. This leads to $v_x \approx 1/3.6$, which inserted into the above equation yields the optimized coordinates: $(I_c^\downarrow, v_x) = (0.81, 0.28)$.

It is noteworthy that we observe, as predicted by the expression for I_c^\uparrow , $I_c(\Omega, I_{ac})$ to be *larger* than the dc-driven system, $I_c(\Omega, I_{ac}) \geq I_c(\Omega, 0) \approx 0.41$. Hence, a transverse ac driving leads to an *enhancement* of the critical current. This is contrary to the case with the ac-current parallel to the dc-current, where the critical current is reduced, *i.e.* $I_c \leq I_c(\Omega, 0) \approx 0.41$.^{5,8,9,10}

The predicted range, ΔS_1 , in I_{dc} of phase-locking, as given by Eq. (31), is investigated through simulations similar to the above study of the critical current. Comparisons between the predicted expression and results of numerical simulations are shown in figure 5a, which displays the largest magnitude of the range in dc current for which phase-locking is observed as a function of the characteristic ratio, $\frac{I_{ac}}{\Omega}$, for different values of Ω in the interval $1 \leq \Omega \leq 3$. Markers represent results of numerical simulations and solid curves represent the corresponding predicted results of Eq. (31). It is obvious that the simulated parameter sets provide very good overall validation of the perturbation analysis, with the larger of the simulated frequencies providing better agreement than the smaller, as expected. However, an observation common to all simulated frequencies is that large deviations from the expected behavior are found for parameter values (Ω and I_{ac}) leading to $J_0(\frac{I_{ac}}{\Omega}) \approx 0$. The reason for this discrepancy is likely due to a dynamical instability, which can be explained by the perturbation analysis above. The average equilibrium position, $\langle \Psi_y \rangle$, of the variable Ψ_y can be observed from Eq. (26) if we write $\Psi_y = \Psi_y^{(0)} + \psi_y$, where $\Psi_y^{(0)}$ is varying slowly in time (much slower than Ω), and ψ_y represents all high frequency (including Ω) contributions ($|\psi_y| \ll 1$). The slow evolution of equation (26) can then be written,

$$2\dot{\Psi}_y^{(0)} + J_0\left(\frac{I_{ac}}{\Omega}\right) \sin \Psi_y^{(0)} = 0. \quad (38)$$

Thus, we find that the stable position of Ψ_y is:

$$\langle \Psi_y \rangle = \begin{cases} 0 & , J_0\left(\frac{I_{ac}}{\Omega}\right) > 0 \\ \pi & , J_0\left(\frac{I_{ac}}{\Omega}\right) < 0 \end{cases}. \quad (39)$$

The consequence of this abrupt transition in Ψ_y is that the locking phase, $\Phi_x^{(0)}$, must experience a similar abrupt transition of π , as can be seen from equation (11). We therefore claim that the apparent discrepancy observed between the numerical simulations and the perturbation theory near the roots of $J_0(\frac{I_{ac}}{\Omega})$, is a result of dynamical instabilities arising from switching the average phase, $\langle \Psi_y \rangle$ between 0 and π .

We finally show the comparisons of the center of the phase-locked step as a function of the characteristic ratio, $\frac{I_{ac}}{\Omega}$, for different values of Ω in the interval $1 \leq \Omega \leq 3$. The predicted behavior, Eq. (32), is subject to the same issues as the predicted range of phase-locking since the origin of both expressions is Eq. (30). Figure 5b shows the offset, $\Delta I_1 = I_1 - \Omega$, between the center of the step, I_1 , and the Ohmic curve. As is the case for the phase-locking range shown in figure 5a, the comparison between numerical simulations (markers) and the corresponding predicted offsets (solid curves) is very good, except for the instabilities near the roots of $J_0(\frac{I_{ac}}{\Omega})$. Notice that the phase-locking analysis leading to the predictions Eqs. (31) and (32) does not depend on the sharp Ψ_y transition between 0 and π . The reason is that this transition provides only a sign change in the effective equations of phase-locking, and the magnitudes of locking range and offset are therefore unaffected as long as $J_0(\frac{I_{ac}}{\Omega}) \neq 0$.

Based on the above presented comparisons between the numerical simulations of critical currents, range of phase-locking and position of the phase-locked step in the IV characteristics of a transversely ac-driven JJA and the corresponding results from simple perturbation analysis, we conclude that the high frequency behavior is well described by the presented analytical treatment.

B. Critical Current and Phase-Locking for intermediate and low Ω

In Fig. 6 we show the critical current behavior for intermediate and low frequencies. For intermediate frequencies (figure 6a) we observe how the critical current, I_c^\dagger , increasingly deviates from the high frequency behavior outlined above. Even so, we notice that the overall behavior of the critical current is qualitatively well described by the analysis leading to equation (21) for $\Omega \geq \frac{1}{2}$. We have, for comparison, included an example of the critical current for the longitudinally ac-driven JJA as an inset. Not surprisingly, decreasing the frequency further (see figure 6b) results in rather large discrepancy between the high frequency analysis of section IIIA and the numerical simulations, and no universal behavior of the critical current as a function of the characteristic ratio, $\frac{I_{ac}}{\Omega}$, can be found. However, we do observe that the critical current does seem to increase quadratically for small I_{ac} .

In Fig. 7 we show the phase-locking range, ΔS_1 , at $v_x = \Omega$ as a function of I_{ac}/Ω for intermediate ($\Omega > 0.5$) and low frequencies ($\Omega < 0.5$). Again, as for the critical current we observe that the intermediate frequency range provides for reasonably good qualitative comparisons between numerical simulations and the high frequency analysis of section IIIA. We have, for comparison, included an example of the comparable range of phase-locking for the longitudinally ac-driven JJA as an inset. A noticeable feature of figure 7a is that the dynamical instability discussed above around $J_0(\frac{I_{ac}}{\Omega}) = 0$ seems to widen as the frequency is lowered. Figure 7b shows how this instability provides for increasing discrepancy between high frequency analysis and numerical simulations. However, we notice that even the very low frequencies retain the basic feature of quadratic growth of the phase-locking range as a function of I_{ac} for small I_{ac} .

C. Dynamics of Phase-Locking

Let us now analyze in detail the dynamics of the voltage responses (increasing and decreasing dc-current) to elaborate on our previous results: critical current hysteresis and windows without transverse phase locking. We calculate IV curves and Lyapunov exponents as a function of I_{ac} and Ω . In order to distinguish between periodic or quasi-periodic dynamics and chaotic dynamics we calculate the maximum Lyapunov exponent, λ , following the standard methods of nonlinear dynamics.^{34,35} This means that a small perturbation, $\vec{\epsilon}(0)$, to the initial condition will displace the new trajectory by an amount $|\vec{\epsilon}(t)| \sim |\vec{\epsilon}(0)|e^{\lambda t}$. The Lyapunov exponent is then defined as

$$\lambda = \lim_{t \rightarrow \infty} \frac{1}{t} \ln \frac{|\vec{\epsilon}(t)|}{|\vec{\epsilon}(0)|} = \lim_{t \rightarrow \infty} \lambda(t).$$

To recognize a chaotic trajectory we evaluate the maximum Lyapunov exponent. If $\lambda > 0$ the trajectory is locally unstable; i.e., initial points that are arbitrarily close to each other are macroscopically separated by the flow after a sufficiently long time and the attractor is chaotic. Negative Lyapunov exponents are obtained when trajectories that start sufficiently close to a subset are attracted to it. Here we will show two particular cases: $I_{ac}/\Omega = 3.0/1.5 = 2$, corresponding to a set of parameters where no hysteresis is obtained, and $I_{ac}/\Omega = 4.05/1.5 = 2.7$, corresponding to the hysteretic regime. In Fig. 8 we plot the IV curves and maximum Lyapunov exponents for $\Omega = 1.5$ and $I_{ac} = 3.0$ (a-b) and $I_{ac} = 4.05$ (c-d). The exponents are estimated from $\lambda \approx \lambda(t)$ after a finite time $t = 1024T$, with $T = 2\pi/\Omega$. For $I_{ac} = 3.0$ we show a range in I_{dc} where a wide transverse phase locking step exists (Fig. 8a), and the corresponding maximum Lyapunov exponent, λ , is shown in Fig. 8b. We see that within the step we have $\lambda < 0$, with the most negative value of λ at the center of the step. Outside the steps, the Lyapunov exponent is nearly equal to zero, $\lambda \lesssim 0$, corresponding to quasiperiodic behavior. A different behavior is obtained for $I_{ac} = 4.05$, shown in Fig. 8c, where we see that the step disappears and thus there is no transverse phase locking in the same I_{dc} range where we find a step in Fig. 8a. The maximum Lyapunov exponent, plotted in Fig. 8d, is small but positive for the I_{dc} range around the expected location of the step, the smallness of λ implies that the dynamics can be either chaotic ($\lambda > 0$) or quasiperiodic ($\lambda = 0$) in this case. The IV curves near the corresponding critical currents are shown as insets. We see that the absence of hysteresis in critical current is associated with the occurrence of transverse phase locking. Inversely, hysteresis in critical current is obtained for approximately the same parameters for which transverse phase locking is absent. This is in agreement with the above analysis that indicates the critical current hysteresis is present in the vicinity of $J_0(\frac{I_{ac}}{\Omega}) = 0$, which is also the location of the dynamical instabilities of the locked phase of the ΔS_1 step.

In summary, around the transverse phase locking step region we can distinguish three different voltage responses: A, B and C, which are indicated in Fig. 8. We now calculate the voltage power spectrum and Poincaré sections to distinguish these three types of dynamical behavior. This way to characterize dynamical behaviors was used before in capacitive rf-biased JJA.^{36,37} We analyze both transverse and longitudinal voltage power spectra. From the

instantaneous transverse voltage we obtain the transverse voltage power spectrum:

$$S_y(\omega) = \left| \frac{1}{T_t} \int_0^{T_t} dt V_y(t) \exp(i\omega t) \right|^2, \quad (40)$$

where $T_t = N_t \Delta t$. From the instantaneous longitudinal voltage, V_x , we obtain the longitudinal voltage power spectrum:

$$S_x(\omega) = \left| \frac{1}{T_t} \int_0^{T_t} dt V_x(t) \exp(i\omega t) \right|^2. \quad (41)$$

For studying the nature of the attractor in the different regimes it is useful to consider a Poincaré section of the phase-space trajectories.³⁴ We consider the stroboscopic Poincaré section of the trajectories in the $d\Phi_x/dt$ vs. $\sin \Phi_x$ plane, recording the values taken by these variables each period of the ac drive. In Fig. 9 we show the power spectra and Poincaré sections for $\Omega = 1.5$ and for the I_{ac} and I_{dc} values corresponding to the A, B and C regimes. For each case we show the longitudinal, $S_x(\omega)$, and transverse, $S_y(\omega)$, voltage power spectra as a function of ω/Ω and their corresponding Poincaré sections. Let us first discuss the case corresponding to the regime B, in which there is transverse phase-locking. This is shown in Fig. 9b for $I_{dc} = 1.66$ and $I_{ac} = 3.0$, which corresponds to the step with mean voltage $v_x = \langle V_x \rangle = \Omega$ (see Fig. 8a, regime B). We see that the longitudinal power spectrum, $S_x(\omega)$, presents a delta-like peak for $\omega = 2\Omega$. Thereby, the first harmonic of longitudinal voltage fluctuations is locked to 2Ω , as expected for this step, since it corresponds to $n = 2$ in the phase-locking condition $\omega_0 = n\Omega$. The phase-locking with a double frequency corresponds to the case when the vortex lattice oscillates in full synchrony with the transverse ac-current, and the ground state repeats itself after one period of the ac drive. In the transverse voltage power spectrum, S_y , there is a sharp peak at Ω . This is characteristic of transverse phase-locking: the dynamics in the transverse direction locks at half the frequency than the dynamics of the longitudinal direction. This is so because in a single period of the ac-drive, $T = 2\pi/\Omega$, the longitudinal component moves forward n steps in the lattice period a , while the transverse component completes only the first half of its oscillation. In Fig. 9e, we show the Poincaré section corresponding to this case in the regime B. The figure shows a very localized Poincaré section since the trajectory always comes back approximately to the same location in phase space in each ac cycle, since the trajectory is periodic (closed orbit).

Now we analyze the case corresponding to the A regime, which is for a current outside the step, $I_{dc} = 1.5$, see Fig. 8a. In this case we see again in $S_x(\omega)$ a peak at 2Ω and in $S_y(\omega)$ a peak at Ω . However, the peaks now have a small broadening, and small amplitude satellite peaks have appeared at neighboring frequencies. This is evidence of another kind of long-term behavior, namely quasiperiodic dynamics. We can corroborate this with the corresponding Poincaré section shown in Fig. 9d. It consists now on a closed one dimensional curve, which means that trajectories wind around on a torus, never intersecting itself and yet never quite closing, typical of a quasiperiodic orbit. We have also looked at the time dependent estimates of the Lyapunov exponent, $\lambda(t)$. We find that $\lambda(t) < 0$ for finite t , but its absolute value tends to zero for long times as $1/t$, consistent with quasiperiodic behavior.

Let us now study the last case, corresponding to regime C. This is done for $I_{dc} = 1.66$ and $I_{ac} = 4.05$ in Fig. 9c. We see that there are broad peaks in the spectrum in both directions, $S_x(\omega)$ and $S_y(\omega)$, and that there is a marked increase in the power spectra for low frequencies. Moreover, in Fig. 9f we show the corresponding Poincaré section which consists on successive points jumping from one region of phase space to another and forming a complex curve, which does not seem to close on itself. It is rather difficult to decide from this plot if it corresponds to a quasiperiodic orbit or to a low dimensional attractor of a weakly chaotic orbit. We have obtained also the time dependent estimate of the Lyapunov exponent also for this case. We find that $\lambda(t) > 0$ for all t , but its magnitude is decreasing with time as $1/t$ as far as we have been able to observe. The fact that $\lambda(t)$ is positive for finite t means that there is a dynamical instability that causes a seemingly chaotic behavior at intermediate times and a large noise as seen in the low frequency power spectrum. However, for long times it is very likely that the system will settle in a quasiperiodic dynamics with $\lambda(t) \rightarrow 0$. In any case, the regime C is very different from the regime A, as can be seen by comparing the power spectra of Fig. 9a and Fig. 9c.

Another view of the dynamics can be obtained by looking at the behavior of the Lyapunov exponent and the noise in the region, where a step is expected, as a function of I_{ac}/Ω . We proceed as follows: for a given I_{ac} , Ω , we compute the set of values of Lyapunov exponents λ and low frequency longitudinal noise $S_0 = \lim_{\omega \rightarrow 0} S_x(\omega)$ that correspond to currents I_{dc} in the region of voltage where a step is expected. (We look at I_{dc} values for which $\Omega - \epsilon < V_x < \Omega + \epsilon$, we consider $\epsilon = 0.005$). We plot the resulting set of values of λ as a function of I_{ac}/Ω in Fig. 10a and the values of S_0 as a functions of I_{ac}/Ω in Fig. 10b. The vertical lines in the plot correspond to the zeroes of $J_0(I_{ac}/\Omega)$. We see clearly that near these values there are windows of dynamical instability where $\lambda \gtrsim 0$ and where the noise S_0 is large. In the regions of phase-locking we find a couple of interesting results that are worth mentioning. (i) The most negative value of the Lyapunov exponent occurs in the middle of the phase-locked step and its magnitude is proportional to the step width ΔS_1 , as given by Eq. (31). (ii) The largest value of the noise S_0 occurs at the edge of the phase-locked step; its magnitude is also proportional to the step width ΔS_1 , as given by Eq. (31).

D. Results for Large JJA

We will now consider the quality of the simple 2×2 model as representing the dynamics of large $N \times N$ JJAs. It is known that collective effects at high currents may come into play. At high currents, the Z_2 symmetry of the ground state can be broken because a driving current can induce domain walls.^{29,30,32} Simulations of IV curves with the RSJ model and free boundary conditions, for $f = 1/2$ and $T = 0$ have reported a chaotic regime at $I > I_c$ related to the motion of domain walls.³⁸ It has been shown that open boundary conditions nucleate domain walls leading to a critical current lower than de analytic value $I_c = 0.35 < \sqrt{2} - 1$ at $T = 0$.³⁹ Moreover, Ciria and Giovannella¹¹ have shown microscopically that different dynamical states are possible for the longitudinal Shapiro steps. Besides the checkerboard ground state configuration, other stable solutions with domain-walls are possible. Then, depending on dc current value and history, domain walls can appear, which are not permitted in the four plaquette model. Therefore, in order to evaluate to what extent the four plaquette model is valid in the transverse ac driven case, we have calculated numerically IV curves for $N \times N$ arrays, for $N = 8, 16, 32, 64$, with the full RSJ model used before in Ref. 27,30. We use periodic boundary conditions in both directions in the presence of an external dc current, I_{dc} , plus a perpendicular ac current, $I_{ac} \sin(\Omega t)$. We solve the dynamical equations with time step $\Delta t = 0.1\tau_J$ ($\tau_J = 2\pi cR_N I_0 / \Phi_0$) and total integration time $t_{\text{int}} = 2^{15}\Delta t$ after a transient $t_{\text{int}}/2$. We calculate IV curves as a function of I_{ac} and Ω , increasing dc current, I_{dc}^\uparrow , from checkerboard ground state at $I_{dc} = 0$ and then decreasing dc current, I_{dc}^\downarrow , from the phase configuration obtained at high current. We use a dc current step $\Delta I_{dc} = 0.01$ to obtain I_c and $\Delta I_{dc} = 0.0001$ to calculate the step width.

One of the relevant results with the four plaquette model is the dependence of the critical current with I_{ac}/Ω for high frequencies, as shown in Fig. 4a and Fig. 6a. We have also calculated I_c as a function of I_{ac}/Ω for high Ω in large JJA arrays. In Fig. 10a we show the case for a particular high frequency value in a 32×32 array. We see that it has the same behavior as observed in the four plaquette model: $I_c(I_{ac}, \Omega) \geq I_c(0, 0)$, ranges of I_{ac}/Ω around the maxima of I_c where there is hysteresis, and a quadratic increase with I_{ac} for $I_{ac}/\Omega \ll 1$. We compare with the analytical results expected for I_c^\uparrow , Eq. (21) and I_c^\downarrow , Eq. (37), which are represented by dot-dashed lines. We see that I_c^\uparrow obtained numerically for a large array is in excellent agreement with the analytical result for the 2×2 system. This is quite reasonable, since I_c^\uparrow corresponds to the limit of stability of the checkerboard ground state, which is well represented by the 2×2 model. On the other hand, the I_c^\downarrow shows some small deviation from the 2×2 result, $I_c^\downarrow(N \times N) \lesssim I_c(2 \times 2)$. Also the range in I_{ac}/Ω where there is hysteresis is bigger in a large system. The current I_c^\downarrow corresponds to the low current limit of stability of the moving (non-zero voltage) state. In large systems, the moving state can have domain walls, as was found in Ref. 29,30, and the presence of domain walls can lead to a lower I_c^\downarrow .

In order to analyze more quantitatively in which I_{ac}/Ω ranges the collective effects could be more relevant, we focus on two cases: case *a* corresponding to values that do not show hysteresis in the critical current in a small system, but are close to the edge of the I_{ac}/Ω range of hysteresis, and case *b* corresponding to values that show hysteresis in the 2×2 system. For each case we calculate the critical current both increasing and decreasing the dc drive, and therefore they correspond to $a \uparrow$, $a \downarrow$, $b \uparrow$ and $b \downarrow$ in Fig. 10a. We show in the inset of Fig. 10a the critical currents obtained for all these cases as a function of system size, N . In case *a*, corresponding to the non-hysteretic region, we see that there is no size effect in $a \uparrow$ up to $N = 64$. Also we see that $a \downarrow = a \uparrow$ for $N \leq 32$, while for $N = 64$ we find that hysteresis has appeared and $a \downarrow < a \uparrow$. In the hysteretic region, case *b*, size dependent critical currents are obtained for $b \downarrow$, while $b \uparrow$ is size independent. Moreover, the amplitude of the hysteresis, $b \uparrow - b \downarrow$ weakly increases with system size.

In Fig. 10b we show the range of phase locking ΔS_1 as a function of I_{ac}/Ω for the 32×32 array. We find that, when there is phase-locking, the numerically obtained ΔS_1 is very accurately described by the analytical result of Eq. (31) for the 2×2 model. In the inset of Fig. 10b we show the size dependence of ΔS_1 for the case marked as *c* in the plot (it corresponds to the same I_{ac}/Ω of case *a* of Fig. 10a). There is no appreciable size dependence. As observed in the simulations of the 2×2 system, we also find here that the phase-locking is lost near the zeros of $J_0(I_{ac}/\Omega)$ due to the presence of dynamical instabilities. Also we observe that the presence of hysteresis in the critical current is nearly coincident with the absence of phase locking. We find that with increasing system size these regimes of dynamical instability are amplified in their extension both in their I_{dc} dependence and in their range of I_{ac}/Ω around the zeros of $J_0(I_{ac}/\Omega)$. This means that the dynamical instabilities detected in the four plaquette system can lead to an increased spatiotemporal chaos in larger systems where collective effects are important.

V. CONCLUSIONS

It is important to point out that there are no trivial connections between vortex dynamics in the fully frustrated JJA and that of a commensurate vortex lattice moving in a rectangular pinning potential in a bulk superconductor.²²

This is so because the London model with vortices interacting through pair potentials apply to JJAs only in the limit of very low vortex density, such that $f = Ha^2/\Phi_0 \ll 1$.²⁷ The fully frustrated case represents, in this last respect, an interesting limit for studying, where the complete phase field, rather than just the positions of vortices, should be taken into account to describe the dynamics.

We have found transverse phase locking steps in fully frustrated JJA. This new type of (fractional) giant phase-locking steps presents marked differences with the well known longitudinal fractional giant Shapiro steps. Particularly, the presence of the transverse ac force increases the critical depinning current with respect to the case without ac drive (or with a longitudinal ac drive). We have analyzed both analytically and numerically the behavior of the steps as a function of ac amplitude I_{ac} and frequency Ω . For $I_{ac}/\Omega \ll 1$, the depinning critical current and the phase-locked step width ΔS_1 for $V = \Omega\hbar/2e$, increase quadratically with I_{ac} . For $I_{ac}/\Omega > 1$ we have found windows of I_{ac}/Ω where depinning is hysteretic and phase locking is destroyed due to dynamical instabilities. The emergence of a weakly chaotic behavior at zero temperature, in a system with non capacitive junctions, is another particular characteristic of transverse phase locking which is absent in longitudinal phase locking in overdamped JJA. Comparing with the behavior of large fully frustrated arrays we have found that transverse phase locking can be well described by an effective four plaquette model, and that collective effects become more important close to the regions of dynamical instability of the four-plaquette model. Our results could be observed experimentally in JJA. In particular, the enhancement of the critical depinning current with a transverse ac drive could be an interesting experimental consequence of the phenomena reported here.

Acknowledgments

We acknowledge discussions with G. Carneiro, H. Pastoriza, C. Reichhardt and D. Shalom. Parts of this work were supported by the Director, Office of Advanced Scientific Computing Research, Division of Mathematical, Information and Computational Sciences of the U.S. Department of Energy under contract number DE-AC03-76SF00098. The work in Argentina was supported by CNEA, Conicet and ANPCyT (PICT99-03-06343).

-
- ¹ Per Bak, *Physics Today*, December 1986, 36.
² S. Shapiro, *Phys. Rev. Lett.* **11**, 80 (1963).
³ A. Barone and G. Paterno, *Physics and applications of the Josephson Effect* (Wiley, New York, 1982).
⁴ Ch. Leeman, Ph. Lerch, and P. Martinoli, *Physica* **126B**, 475 (1984).
⁵ S. P. Benz, M. S. Rzchowski, M. Tinkham, and C. J. Lobb, *Phys. Rev. Lett.* **64**, 693 (1990); *Physica B* **165-166**, 1645 (1990).
⁶ H. C. Lee, R. S. Newrock, D. B. Mast, S. E. Hebboul, J. C. Garland, and C. J. Lobb, *Phys. Rev. B* **44**, 921 (1991); S. E. Hebboul and J. C. Garland, *Phys. Rev. B* **43**, 13703 (1991); *Phys. Rev. B* **47**, 5190 (1993).
⁷ K. H. Lee, D. Stroud, and J. S. Chung, *Phys. Rev. Lett.* **64**, 962 (1990); K. H. Lee and D. Stroud, *Phys. Rev. B* **43**, 5280 (1991).
⁸ J.U. Free, S. P. Benz, M. S. Rzchowski, M. Tinkham, and C. J. Lobb and M. Octavio, *Phys. Rev. B* **41**, 7267 (1990).
⁹ M.S. Rzchowski, L.L. Sohn, and M. Tinkham, *Phys. Rev. B* **43**, R8682 (1991).
¹⁰ M. Octavio, J.U. Free, S.P. Benz, R.S. Newrock, D.B. Mast, C.J. Lobb, *Phys. Rev. B* **44**, 4601 (1991).
¹¹ J. C. Ciria and C. Giovanella, *J. Phys. Cond. Matt.* **8**, 3057 (1996); J. C. Ciria and C. Giovanella, in *Macroscopic Quantum Phenomena and Coherence in Superconducting Networks*, Ed. C. Giovannella and M. Tinkham (World Scientific, Singapore, 1995), p.301.
¹² D. Domínguez, J. V. José, A. Karma and C. Wiecko, *Phys. Rev. Lett.* **67**, 2367 (1991); D. Domínguez and J. V. José, *Phys. Rev. Lett.* **69**, 514 (1992); *Phys. Rev. B* **48**, 13717 (1993), and *Int. J. Mod. Phys. B* **8**, 3749 (1994).
¹³ C. Giovanella, F. Ritort and A. Gianelli, *Europhys. Lett.* **29**, 419 (1995).
¹⁴ L. Van Look, E. Rosseel, M. J. Van Bael, K. Temst, V. V. Moshchalkov, and Y. Bruynseraede, *Phys. Rev. B* **60**, R6998 (1999).
¹⁵ C. Reichhardt, R. T. Scalettar, G.T. Zimányi, and N. Grønbech-Jensen, *Phys. Rev. B* **61**, R11914 (2000)
¹⁶ P. Martinoli, O. Daldina, C. Leemann, and E. Stocker, *Solid State Commun.* **17**, 205 (1975).
¹⁷ N. Kokubo, R. Besseling, V. M. Vinokur and P. H. Kes, *Phys. Rev. Lett.* **88**, 247004 (2002).
¹⁸ G. Grüner, *Rev. Mod. Phys.* **60**, 1129 (1988); S. Bhattacharya, J. P. Stokes, M. J. Higgins, and R. A. Klemm, *Phys. Rev. Lett.* **59**, 1849 (1987); M. J. Higgins, A. A. Middleton, and S. Bhattacharya, *ibid.* **70**, 3784 (1993); S. N. Coppersmith and P. B. Littlewood, *ibid.* **57**, 1927 (1986); A. A. Middleton, O. Biham, P. B. Littlewood, and P. Sibani, *ibid.* **68**, 1586 (1992).
¹⁹ A. T. Fiory, *Phys. Rev. Lett.* **27**, 501 (1971).
²⁰ J. M. Harris, N. P. Ong, R. Gagnon, and L. Taillefer, *Phys. Rev. Lett.* **74**, 3684 (1995).
²¹ A. B. Kolton, D. Domínguez, N. Grønbech-Jensen, *Phys. Rev. Lett.* **86**, 4112 (2001).
²² C. Reichhardt, A. B. Kolton, Daniel Domínguez and N. Grønbech-Jensen, *Phys. Rev. B* **64**, 134508 (2001); C. Reichhardt and C. J. Olson, *Phys. Rev. B* **65**, 174523 (2002).

- ²³ A. B. Kolton, D. Domínguez, N. Grønbech-Jensen, Phys. Rev. B **65**, 184508 (2002).
- ²⁴ A. E. Koshelev and V. M. Vinokur, Phys. Rev. Lett. **73**, 3580 (1994); S. Scheidl and V. M. Vinokur, Phys. Rev. B **57**, 13800 (1998); T. Giamarchi and P. Le Doussal, Phys. Rev. Lett. **76**, 3408 (1996); P. Le Doussal and T. Giamarchi, Phys. Rev. B **57**, 11356 (1998); L. Balents, M. C. Marchetti and L. Radzihovsky, *ibid.* **57**, 7705 (1998).
- ²⁵ K. Moon *et al.*, Phys. Rev. Lett. **77**, 2778 (1996); S. Ryu *et al.*, *ibid.* **77**, 5114 (1996); N. Grønbech-Jensen *et al.*, *ibid.* **76**, 2985 (1996); C. Reichhardt *et al.*, *ibid.* **78**, 2648 (1997); D. Domínguez *et al.*, *ibid.* **78**, 2644 (1997); C. J. Olson *et al.*, *ibid.* **81**, 3757 (1998); D. Domínguez, *ibid.* **82**, 181 (1999); A. B. Kolton, D. Domínguez, and N. Grønbech-Jensen, Phys. Rev. Lett. **83**, 3061 (1999); H. Fangohr *et al.*, Phys. Rev. B **63**, 064501 (2001); K. Bassler *et al.*, *ibid.* **64**, 224517 (2001).
- ²⁶ C. J. Olson and C. Reichhardt, Phys. Rev. B **61**, R3811 (2000); H. Fangohr *et al.*, *ibid.* **63**, 064501 (2001).
- ²⁷ V. I. Marconi and D. Domínguez, Phys. Rev. Lett. **82**, 4922 (1999); Phys. Rev. B **63**, 174509 (2001).
- ²⁸ A. B. Kolton, D. Domínguez, N. Grønbech-Jensen, Phys. Rev. Lett. **83**, 3061 (1999); A. B. Kolton, D. Domínguez, C.J. Olson, N. Grønbech-Jensen, Phys. Rev. B **62**, R14657 (2000).
- ²⁹ N. Grønbech-Jensen, A. R. Bishop, F. Falo, and P. S. Lomdahl, Phys. Rev. B **46**, 11149 (1992).
- ³⁰ V. I. Marconi and D. Domínguez, Phys. Rev. Lett. **87**, 017004 (2001).
- ³¹ S. Teitel and C. Jayaprakash, Phys. Rev. B **27**, 598 (1983), Phys. Rev. Lett. **51**, 1999 (1983).
- ³² K. K. Mon and S. Teitel, Phys. Rev. Lett. **62**, 673 (1989).
- ³³ S. P. Benz, M. S. Rzchowski, M. Tinkham, and C. J. Lobb, Phys. Rev. B **42**, 6165 (1990).
- ³⁴ Steven H. Strogatz, *Nonlinear dynamics and Chaos*, Perseus Books, Cambridge, Massachusetts, 1998.
- ³⁵ I. Shimada and T. Nagashima, Prog. Theor. Phys. **61**, 1605 (1979).
- ³⁶ R.L. Kautz and R. Monaco, J. Appl. Phys. **57**, 875 (1985).
- ³⁷ Thomas Hagenaaers, PhD Thesis (1995), Universiteit Utrecht.
- ³⁸ F. Falo, A. R. Bishop, and P. S. Lomdahl, Phys. Rev. B **41**, 10983 (1990).
- ³⁹ B. J. Kim and P. Minnhagen, Phys. Rev. B **61**, 7017 (2000).

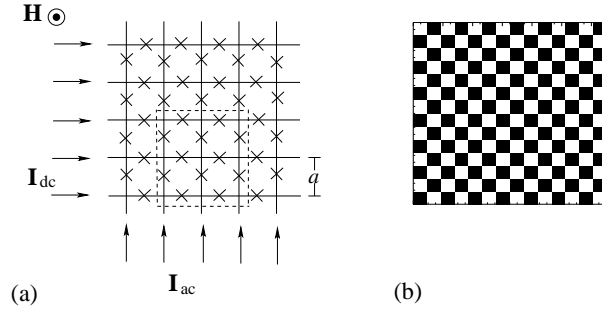


FIG. 1: (a) Schematic JJA showing driving currents, and the repeated two-junction by two-junction superlattice unit cell in the ground state. (b) Ground state “checkerboard” vorticity for $f = Ha^2/\Phi_0 = 1/2$. Black squares represent plaquettes with one vortex, white squares represent plaquettes without vortices.

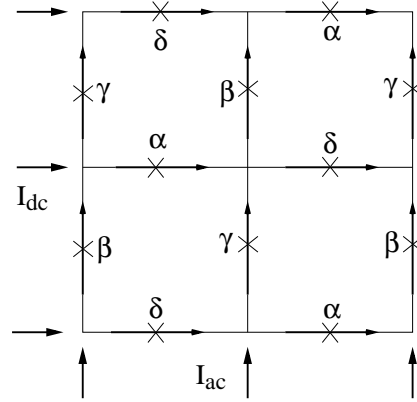


FIG. 2: Square four-plaquette model, being α , β , γ , δ , the gauge-invariant phase differences.

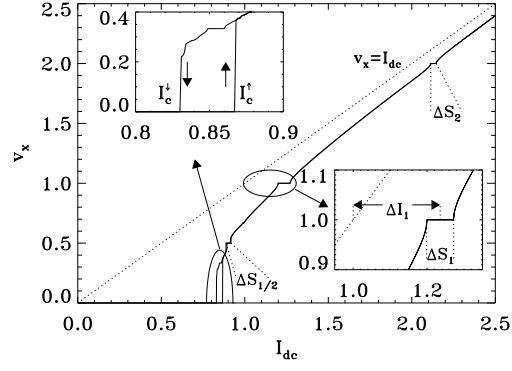


FIG. 3: IV curve of a 2×2 JJA for $I_{ac} = 2.3$ and $\Omega = 1$, showing transverse phase locking and critical currents. Inset shows a detail of the hysteresis around the critical current.

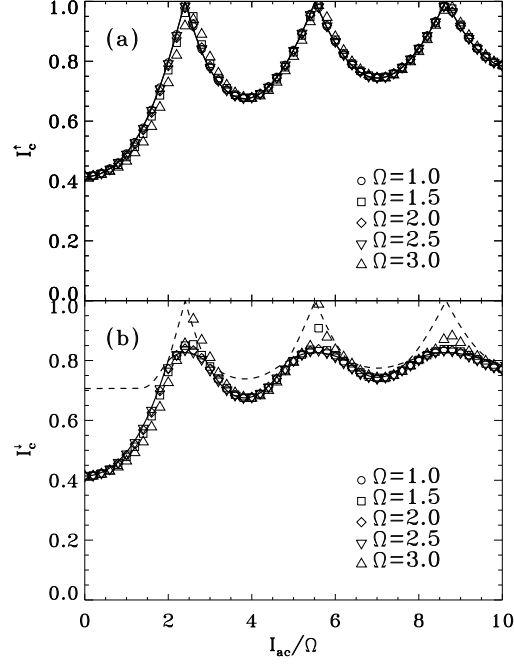


FIG. 4: Critical current, I_c , of a 2×2 JJA vs ac-amplitude and frequency, I_{ac}/Ω for high frequencies, $\Omega \geq 1$. The hysteresis of the critical current is demonstrated by (a) the critical current, I_c^\uparrow , switching from zero to non-zero voltage state, and (b) the critical current, I_c^\downarrow , switching from non-zero to zero voltage states. See Figure 3. Markers are results of numerical simulations and lines are the corresponding predictions: (a) equation (21); (b) dashed curve is the maximum of equations (21) and (37), while the solid curve is the minimum of the two. The critical current, I_c^\downarrow , is predicted to follow the solid curve.

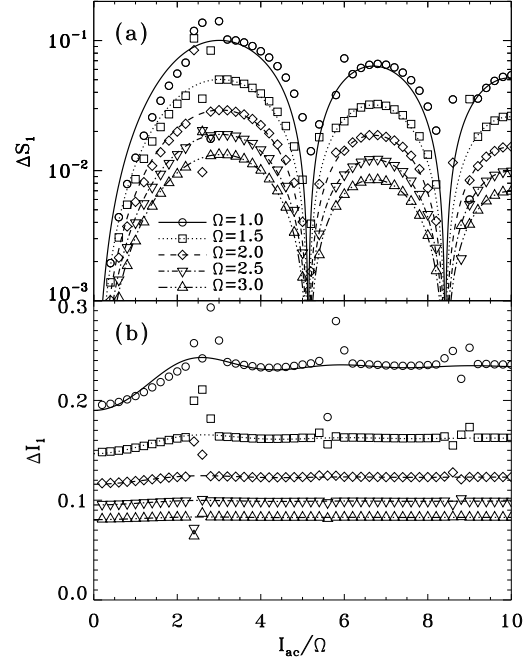


FIG. 5: Phase-locking of a 2×2 JJA at $V_x = \Omega$. Markers are results of numerical simulations and lines are the corresponding predictions of equations (31) and (32). (a) Phase-locking range in dc current. (b) Offset of the phase-locked step relative to the Ohmic curve. See Figure 3.

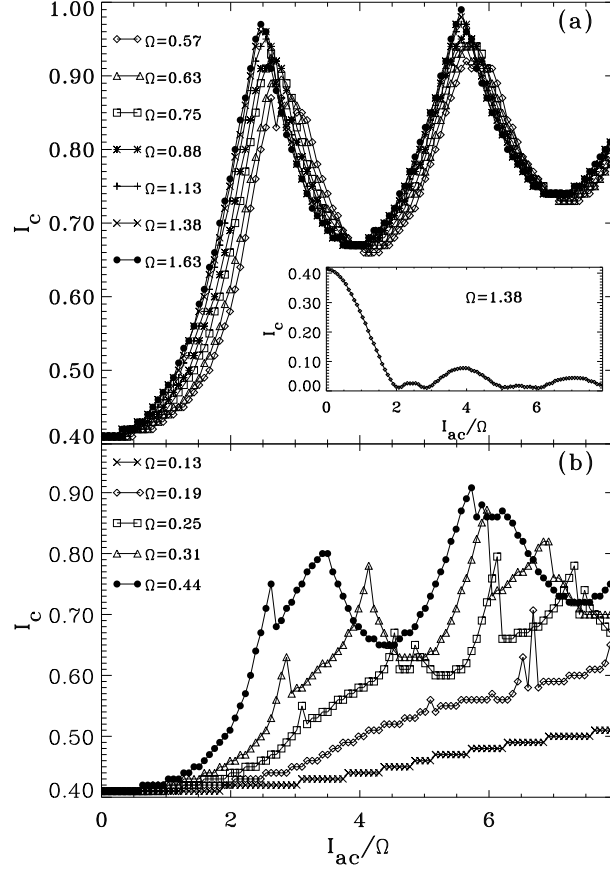


FIG. 6: Critical current, I_c^\uparrow , as a function of ac-amplitude and frequency, I_{ac}/Ω for intermediate frequencies, $\Omega > 0.5$ (a) and for low frequencies, $\Omega < 0.5$ (b). Inset: Comparison with longitudinal ac-drive for $\Omega = 1.38$.

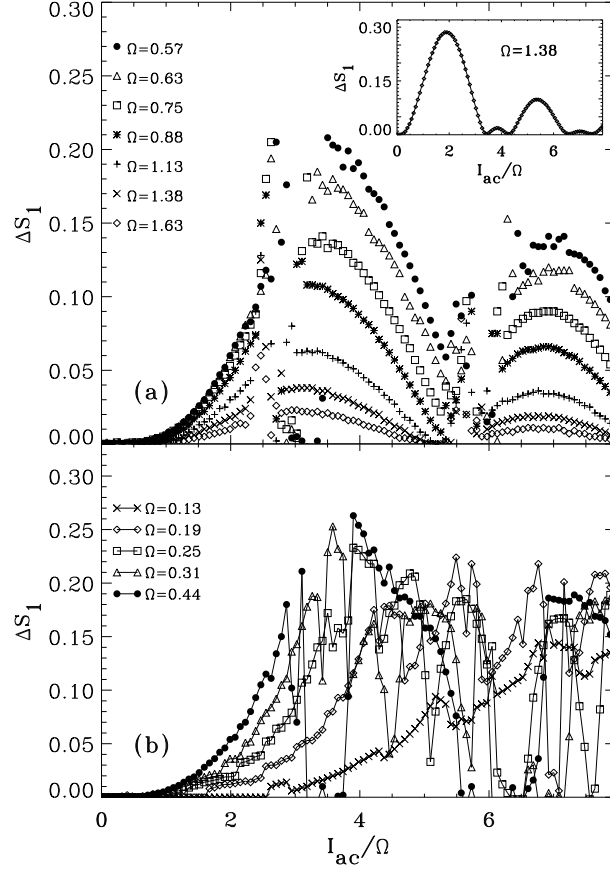


FIG. 7: First integer step width, ΔS_1 , vs ac-amplitude and frequency, I_{ac}/Ω for intermediate frequencies, $\Omega > 0.5$ (a) and low frequencies, $\Omega < 0.5$ (b). Inset: Comparison with longitudinal ac-drive for $\Omega = 1.38$.

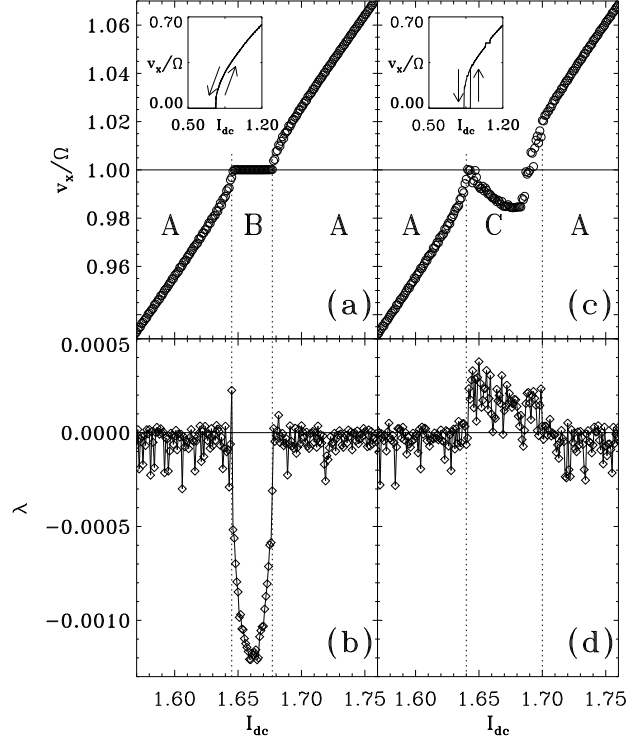


FIG. 8: IV curves for $\Omega = 1.5$ and their corresponding Lyapunov exponents, λ : (a) Part of IV curve with phase locking step for $I_{ac} = 3.0$. Inset: detail of IV curve near the critical current. No hysteresis in I_c is observed. (b) λ for $I_{ac} = 3.0$. (c) IV curve for $I_{ac} = 4.05$, no phase locking step is observed. Inset: detail of IV near the critical current: hysteresis in I_c . (d) λ for $I_{ac} = 4.05$.

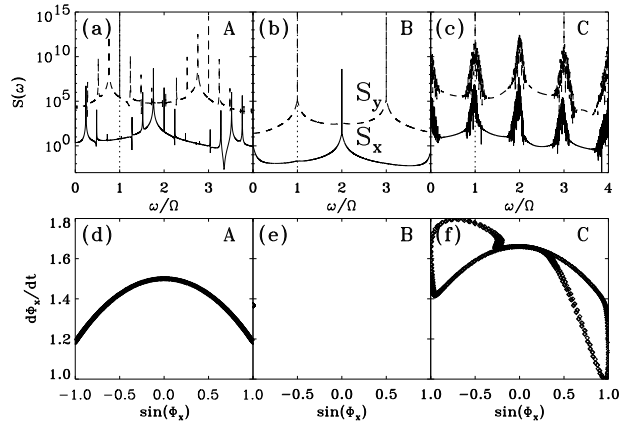


FIG. 9: Voltage power spectra and Poincaré sections for $\Omega = 1.5$ in different I_{dc} regimes: A, B and C (see Fig. 8. (a) Transverse, S_y , and longitudinal, S_x , power spectra for $I_{dc} = 1.5$ and $I_{ac} = 3.0$. A regime. (b) $I_{dc} = 1.66$ and $I_{ac} = 3.0$. B regime. (c) $I_{dc} = 1.66$ and $I_{ac} = 4.05$. C regime. (d),(e) and (f) are the corresponding Poincaré sections. Power spectrum S_x is plotted displaced in the y -axis for clarity.

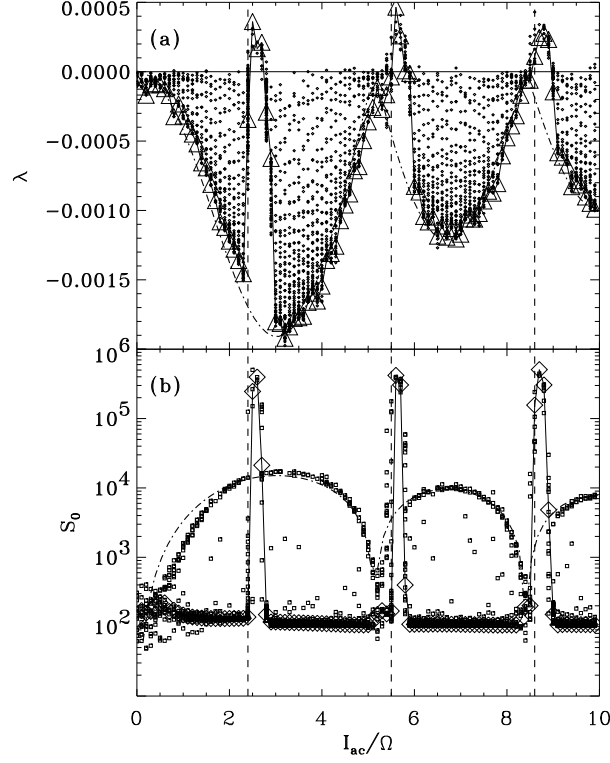


FIG. 10: Lyapunov exponents λ and low frequency noise S_0 for currents I_{dc} giving voltages near $V = \Omega$ plotted as a function of I_{ac}/Ω . Vertical dashed lines correspond to the zeros of $J_0(I_{ac}/\Omega)$. (a) Lyapunov exponents. Symbol \triangle indicates value of λ at the center of the phase-locked step. Dot-dashed line: curve proportional to $\Delta S_1(I_{ac}/\Omega)$ as given by Eq. (31). (b) Low frequency noise. Symbol \diamond indicates value of S_0 at the center of the phase-locked step. Dot-dashed line: curve proportional to $\Delta S_1(I_{ac}/\Omega)$ as given by Eq. (31).

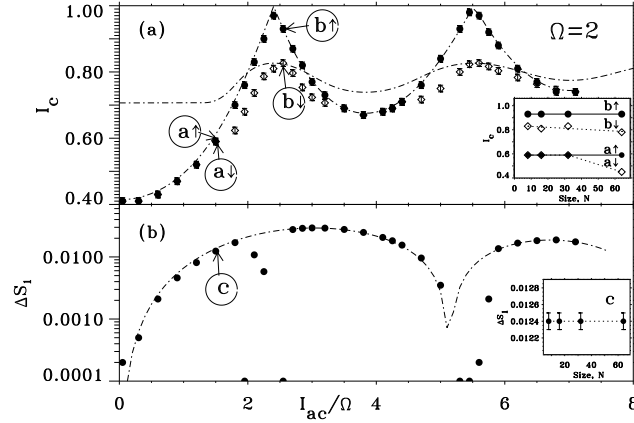


FIG. 11: Critical currents I_c and step widths ΔS_1 obtained from numerical simulation in large arrays (32×32 junctions) as a function of I_{ac}/Ω . (a) I_c obtained increasing I_{dc} (I_c^\uparrow , \bullet) and decreasing I_{dc} (I_c^\downarrow , \diamond). Dot-dashed lines show the analytical results of Eq. (21) and Eq. (37). Inset shows the size dependence of I_c^\uparrow and I_c^\downarrow for system of size $N \times N$, corresponding to the cases a and b indicated in the plot. (b) Width of the first integer phase-locked step ΔS_1 , obtained numerically for a 32×32 array: \bullet , and analytical result of Eq. (31): dot-dashed line. Inset shows size dependence of ΔS_1 for the case c shown in the plot.